ADVANCED ENERGY MATERIALS
www.advenergymat.de

Understanding Boron Chemistry as the Surface Modification and Electrolyte Additive for Co-Free Lithium-Rich Layered Oxide

Na Ri Park, Minghao Zhang, Bing Han, Weikang Li, Kun Qian, HongNam Nguyen, Shinichi Kumakura, and Ying Shirley Meng**

Lithium-rich layered oxide (LRLO) stands out as a highly promising cathode material for the next generation of Li-ion batteries, owing to its exceptional lithium storage capacity. The absence of cobalt in LRLO's composition provides an additional advantage, enabling cost-effective production and thereby improving the feasibility of large-scale manufacturing. Despite these promising attributes, LRLO has encountered challenges related to poor cycling performance and severe voltage decay, impeding its practical application. In addressing these challenges, a surface modification technique involving lithium borate (LBO) is employed through a dry coating method. The LBO-coated LRLO exhibits a uniform surface layer with a thickness of 15 nm. Furthermore, the performance of LBO-coated LRLO in a full cell is synergistically enhanced when combined with lithium bis(oxalato)borate (LiBOB) as an electrolyte additive. A discharge capacity retention of 82% is achieved after 400 cycles at room temperature. These substantial improvements are attributed to the continual reaction between boron species on the LRLO cathode surface and PF_6^- anions in the electrolyte. This reaction generates BF_4^- and suppresses HF acid formation during the high voltage charging process, demonstrating LRLO's potential for practical implementation.

1. Introduction

Li-ion batteries have been extensively investigated, particularly in the context of emerging applications such as electric vehicles (EVs), hybrid electric vehicles (HEVs), portable electronic devices, and energy storage systems. These applications require advanced lithium storage capacity, increased energy density (calculated as the product of specific capacity and average operating voltage), and prolonged battery cycle performance.[1] The ongoing progress in battery systems that meet these demanding requirements underscores the critical nature of cathode development, as the cathode is a key component in Li-ion batteries. In pursuit of this objective, LRLO emerges as a promising candidate for the cathode material.[2] A notable characteristic of the LRLO cathode material is the remarkable reversible capacity of 250 mAh g^{-1} within the voltage range of 2.0 to 4.7 V.[3] Importantly, the incorporation of cost-effective manganese as a substitute for the more expensive nickel and cobalt elements holds significant potential for reducing production costs.[4]

The practical implementation of LRLO is hindered by capacity degradation and voltage decay observed in full cell performance, particularly at high voltages.[5] The elevation of the operating voltage introduces undesirable outcomes, including cathode–electrolyte interfacial reactions, structural transformations, and the formation of lower-voltage redox couples.[6] These effects are posited to initiate at the cathode surface, progressively extending into the bulk over successive cycles.[7] It is acknowledged that the distinctive characteristic of LRLO is oxygen redox activation at high voltages (>4.5 V vs Li/Li^+).[8] This activation gives rise to a cascade of issues during cycling: irreversible oxygen loss, the generation of oxygen vacancies on the surface, migration and dissolution of transition metals, and the redeposition of transition metals on both cathode and anode surfaces.[9]

Extensive efforts have been directed toward mitigating capacity and voltage decay in LRLO through the implementation of cathode surface modifications.[10] This strategic focus arises from the recognition that all pertinent parasitic reactions manifest most

N. R. Park, M. Zhang, B. Han, W. Li, K. Qian, Y. S. Meng
Department of NanoEngineering
University of California San Diego
La Jolla, CA 92093, USA
E-mail: miz016@uchicago.edu; shirleymeng@uchicago.edu
H. Nguyen, S. Kumakura
Umicore
Entrance 1A RBM-PCCa
Watertorenstreet 37A, Olen 2250, Belgium
Y. S. Meng
Pritzker School of Molecular Engineering
The University of Chicago
Chicago, IL 60637, USA

The ORCID identification number(s) for the author(s) of this article can be found under https://doi.org/10.1002/aenm.202401968

DOI: 10.1002/aenm.202401968

actively at the cathode's surface. Diverse methodologies for modifying the surface of LRLO cathode material have been explored, including the wet coating method,[11] atomic layer deposition (ALD),[12] and solution-processable method.[13] A sol–gel based wet coating method, involving the dissolution of $Al(NO_3)_3{\cdot}9H_2O$ and NH_4F in deionized water, was employed by Zhao et al. to establish stable integrated layered-spinel structures.[11] However, the wet coating method utilizing water requires additional chemical infrastructure, including explosion-proof facilities, complicating the commercialization process. Furthermore, the rate capability reported needs to be verified in full cells. X. Zhang et al. utilized the spray pyrolysis process, employing the ALD method, to coat the cathode surface with a very thin layer of Al_2O_3, ≈2–3 nm in thickness. This coating significantly improved the initial Coulombic efficiency and cycling performance of the coin half-cell. However, it also led to a ≈10% decrease in the initial discharge capacity compared to the uncoated cathode, indicating a lithium inventory loss through the coating.[12] S. Kim et al. coated the surface of LRLO with polydopamine (PDA), an oxygen radical scavenger, to form a chemically protective layer, demonstrating an 82% retention in coin half-cell cycling after 200 cycles at room temperature. The use of a self-polymerizing solution impregnation technique for coating poses challenges for mass production due to the necessity of filtering powder during the coating process and subsequent washing with ethanol and deionized water.[13]

Another approach employed for cathode surface treatment is the dry coating method, wherein a solid phase identical to that of the cathode material is utilized, thereby eliminating any heterogeneity between the cathode and the coating material.[14] Notably, the mass production of dry coating is streamlined, involving the straightforward addition of the coating material during the mixing process, without necessitating supplementary infrastructure for commercialization. Consequently, the present study endeavors to advance the properties of the cathode toward commercial viability through the implementation of the dry coating method for surface treatment.

Along with determining the surface modification method, the choice of an appropriate surface modification material is pivotal in achieving performance improvements. A large number of compounds have been investigated, such as fluorides,[15] phosphates,[16] and oxides.[11,12] Fluorides involve the partial doping of F^- into the surface lattice of the oxide, enhancing surface conductivity. However, fluorides have traditionally been utilized in high-Ni cathode materials where excess lithium is prevalent on the surface.[17] Phosphates are also known for their ease of reaction with excess lithium and the absorption of water in the electrolyte.[18] While Li_3PO_4 is preferred due to its ionic conductivity, in the high working voltage range of LRLO, it can readily react with free protons. This reaction leads to the formation of H_3PO_4, consequently inducing a shift in the cell environment toward a deleterious acidic state. Oxides are electrochemically stable materials,[19] generally exhibiting low electrical conductivity, thereby minimizing parasitic reactions of the cathode materials with the electrolyte. Moreover, the versatility in designing various oxides provides flexibility to tailor properties in accordance with specific requirements. Various oxides, such as Li_2ZrO_3,[20] Li_3PO_4,[21] AlF_3,[15] $MgPO_4$,[22] CeO_2,[23] and Al_2O_3[24] have been applied for the surface modification of LRLO to improve cycling stability. Nevertheless, these published results encounter challenges in mitigating the initial irreversible capacity loss, and the application of such inactive oxides as coatings may potentially diminish the reversible capacity.

In this work, we applied surface modification to Co-free LRLO ($Li_{1.222}Ni_{0.349}Mn_{0.651}O_2$) using a dry coating process with LBO based on an organic nano-sized boron precursor. LBO coating materials are introduced as 1) it protects the surface lattice oxygen of LRLO, reducing the exacerbated generation of H_2O and free protons at high voltage; 2) it also reacts with PF_6^- to form thermodynamically stable BF_4^-, mitigating the generation of HF acid in the electrolyte. The quality of surface modification was assessed through electron energy loss spectroscopy (EELS) obtained via scanning transmission electron microscopy (STEM). Our analysis revealed the 15 nm uniform distribution of LBO coating on the LRLO surface, resulting in a significant improvement in cycling stability and mitigation of voltage decay in LRLO/graphite full cells featuring a 3 mAh cm^{-2} areal capacity. These findings have the potential to guide the design of surface modification layers for high-voltage cathode materials and inform the utilization of boron-based electrolyte additives in future applications.

2. Results and Discussion

2.1. LBO Dry Coating Optimization and Cycling Stability Improvement

The dry coating method involves physically mixing powder-form LBO precursors with LRLO in the desired weight percentage and calcination of the blended powder. The detailed LRLO sample information is provided in the Experimental section. The LBO precursors were synthesized through a polyol process, as described in our previous work.[14] The synthesized precursors are organic soft materials featuring boron as a functional group along their C—H backbone (Figure S1a, Supporting Information). Upon mixing, chemical bonding, such as B—H, O—H, and C—H, is established on the LRLO surface. After calcination, it is anticipated that most of the C—H backbone chains will be removed. However, the presence of boron bonding on the LRLO surface can be confirmed. This is evident as both the stretching and bending modes of B—H bonding, absent in pristine LRLO, become distinctly observable after calcination. The resulting chemical bonding, as illustrated in Figure S1b (Supporting Information), plays crucial roles in facilitating conformal contact between the precursor and the core material. These attributes emphasize the unique advantages associated with employing polyol precursors for the dry coating process, including enhanced adhesion due to the functional group, as well as flexibility and plasticity. The critical variables for the mixing and calcination step were then optimized, as shown in Figure S2 (Supporting Information). When the mixing time exceeds 20 min (Figure S3d, Supporting Information), secondary particles break apart. Conversely, mixing for less than 5 min (Figure S3a,b, Supporting Information) reveals agglomeration of LBO precursors. Vigorous mixing for an extended period can impose stress on LRLO, necessitating appropriate mixing conditions. It was determined that mixing for 10 min at 1000 rpm induces the most uniform mixing while simultaneously maintaining the secondary particle of LRLO. After blending the powder, calcination is carried out to decompose the organic functional group within the precursor, thereby yielding the LBO

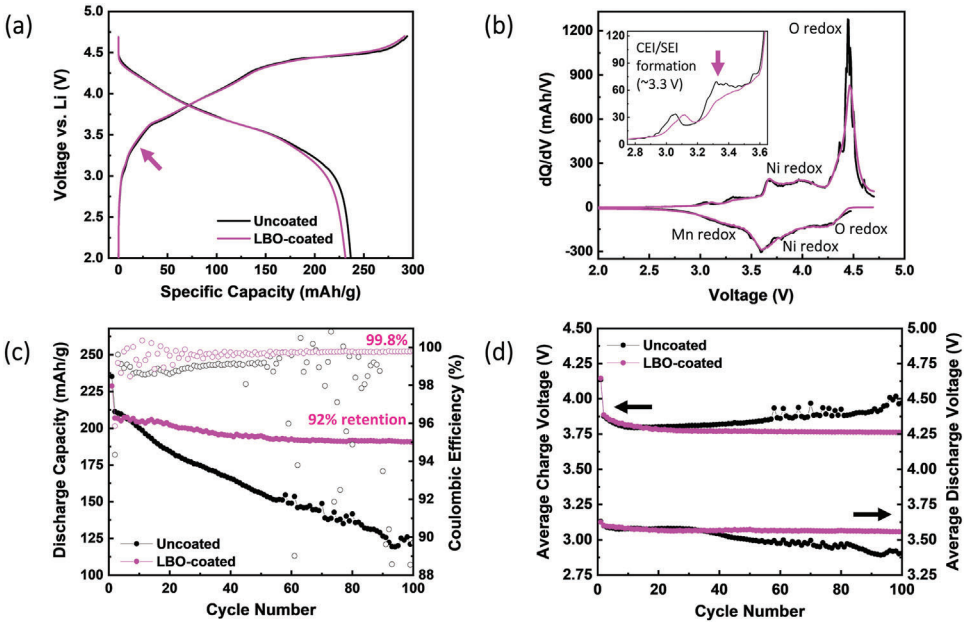

Figure 1. a) Voltage profiles from the uncoated and LBO-coated LRLO/graphite full cell with b) the corresponding dQ/dV plot. The voltage window of both full cells is 2.0–4.7 V at a current rate of C/20 for the formation cycle (1 C = 270 mAh g^{-1}). c) Full cells cycling performances with d) the average charge and discharge voltage in the 2.0–4.55 V window at a current rate of C/10.

coating layer. As shown in Figure S2 (Supporting Information), optimal conditions for the calcination step are achieved when the surface modification appears uniformly, and LBO precursors are no longer visible. This optimal calcination condition with a dwell temperature of 600 °C and a dwell time of 10 h is further verified through electrochemical evaluations (Figure S4, Supporting Information). Another critical variable in this study is the amount of LBO coating. STEM-EELS mapping (Figure S5a, Supporting Information) reveals a boron layer ≈4 nm thick for the 1 wt.% LBO surface modification, which is insufficient to fully cover the cathode surface. The 4 wt.% LBO coating shows clustering of boron species on the cathode surface (Figure S5b, Supporting Information). In contrast, STEM-EELS mapping confirms that the 2 wt.% LBO coating achieves optimal coverage and uniformity (Figure 2a). Electrochemical evaluations were then applied to the coated samples with various weight ratios. As shown in Figure S6a (Supporting Information), the initial capacity drops for 1 and 2 wt.% coatings remain within acceptable values, whereas the 4 wt.% coating results in a capacity loss of 17%. Moreover, during C/10 rate cycling (Figure S6b, Supporting Information), the 1 wt.% LBO-coated LRLO exhibits improved capacity retention compared to the uncoated LRLO; however, this improvement is not comparable with the 2 wt.% sample after ≈50 cycles, indicating that the 1 wt% of LBO coating amount is insufficient. The 4 wt.% LBO-coated LRLO displays a rapid decay in discharge capacity after ≈20 cycles. These results indicate that the amount of LBO coating is crucial for both initial capacity and cycling stability, with 2 wt.% identified as the optimal amount. We confirmed that there was no reduction in electrical conductivity at the electrode level after the surface modification. This is supported by 2-point probe analysis of electrode conductivity with an areal loading of 3 mAh cm^{-2} (Table S1, Supporting Information). Cross-sectional SEM-EDS (Scanning Electron Microscopy with Energy Dispersive X-ray Spectroscopy) analysis in Figure S7 (Supporting Information) has also confirmed that there is no difference in the distribution of conducting carbon additives with and without the LBO surface modification. The similarity in electrical conductivity, combined with the uniformly distributed carbon additives, suggests that the percolation behavior of the electrical conducting agent is nearly identical.

The LBO-coated LRLO exhibits a similar voltage profile (**Figure 1a**) with little capacity loss compared with the uncoated cathode during the formation cycle in full cell. The dQ/dV plots reveal a lower peak intensity for LBO-coated LRLO in the voltage range associated with electrode/electrolyte interphase formation, ≈3.3 V (inset of Figure 1b). The uncoated LRLO shows a continuous decrease in capacity from the beginning of the cycling (Figure 1c). In contrast, LBO-coated LRLO demonstrates ≈92% capacity retention after 100 cycles in full cell. The average charge and discharge voltage plot (Figure 1d) substantiates the role of LBO surface modification on LRLO not only in improving capacity retention but also in ameliorating voltage decay. It is evident that LBO surface modification enhances long-term cycling performances. Figure S8 (Supporting Information) shows that the capacity retention of the uncoated LRLO improved from ≈26% after 500 cycles to ≈63% with just the LBO surface modification.

2.2. LBO Coating Chemistry and Durability

The electrochemical assessment confirmed the effect of the surface modification. To further validate these results, an examination of the presence of boron on the cathode surface was conducted. Mixing LRLO and LBO precursors confirms the presence of relatively lighter material on the cathode surface (Figure S9b, Supporting Information). After calcination, both

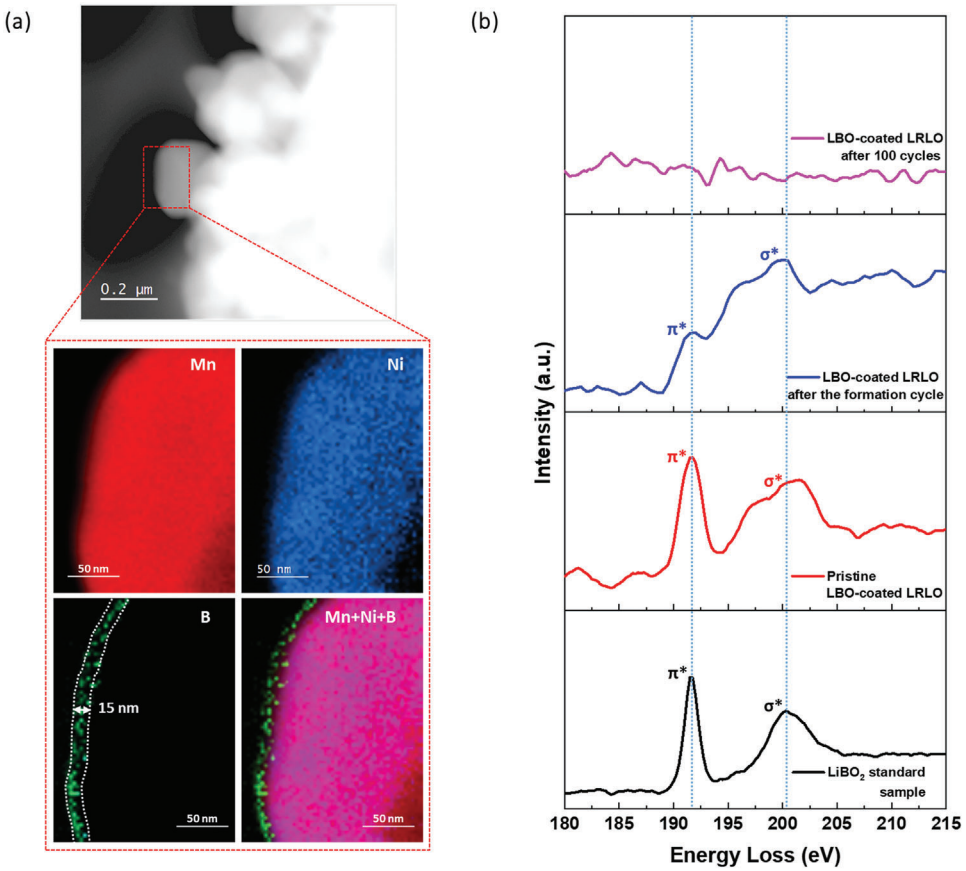

Figure 2. STEM-EELS mapping results of a) LBO-coated LRLO obtained with the optimal dry coating parameters. b) STEM-EELS spectra of boron K-edge for examining the changes in LBO under different electrochemical states and $LiBO_2$ standard sample for comparison.

high-magnification views of the cathode surface (Figure S9c, Supporting Information) and overall observations at low magnification (Figure S9e, Supporting Information) did not exhibit evidence of the coating materials. This observation strongly suggests that the surface modification material, LBO, has undergone a reaction with the cathode surface or beyond. Due to LRLO's polycrystalline nature, assessing coating uniformity in SEM-backscattered electrons (BSE) mode posed challenges. In particular, boron chemistry makes it difficult to confirm the coating uniformity using EDS analysis. The boron layer was then distinctly discerned on the cathode surface through STEM-EELS analysis (**Figure 2**a). Elemental mapping verified the partial diffusion of elements toward the cathode subsurface. This observation indicates a modification in the chemical environment between transition metals and boron, suggesting their influence on improving electrochemical performances.

In order to check the durability of the LBO coating layer and understand its chemical environment, STEM-EELS analysis was conducted on the cathode after the first formation cycle in the full cell. The boron coating layer was still present on the cathode surface after the formation cycle (Figure S10, Supporting Information), albeit in a different chemical environment. Figure 2b compares the EELS spectra of the B K-edge from the surface of the LBO-coated cathode before and after electrochemical cycling. The measured near-edge structure for the $LiBO_2$ standard sample is characterized by a sharp peak at 192 eV associated with transitions to antibonding π^* orbitals, and a broad feature at ≈201 eV originated from σ^* orbitals. At the pristine state, the LBO coating layer closely matches the spectrum from the $LiBO_2$ standard sample, while after the formation cycle, the change in the relative peak intensity is observed. Prior literature[25,26] suggests that the presence of elements such as Ni, Co, and Zn as impurities in boron-based glass can affect the relative peak intensity. Therefore, boron may further diffuse into the transition metal layers during the formation process, which is confirmed through the boron K-edge EELS mapping in Figure S10 (Supporting Information). Following 100 cycles, no boron signal is detected in the boron K-edge spectrum, implying the absence of LBO species on the cathode surface and their reactivity with the electrolyte.

To gain a clear mechanism understanding on the improved full cell performance, tracking boron is essential not only on the cathode but also on the graphite anode. As shown in **Figure 3**a, the presence of a boron layer on the graphite surface with a thickness of up to 15 nm was confirmed after the formation cycle. The layer is thin but uniform and clearly present across the entire surface of the anode, as further confirmed by STEM-EELS spectra analysis (Figure 3b). The peak positions and intensity ratios observed on the anode surface were identical to those observed on the cathode surface after the formation cycle. These observations indicate that the boron initially present on the cathode surface migrates

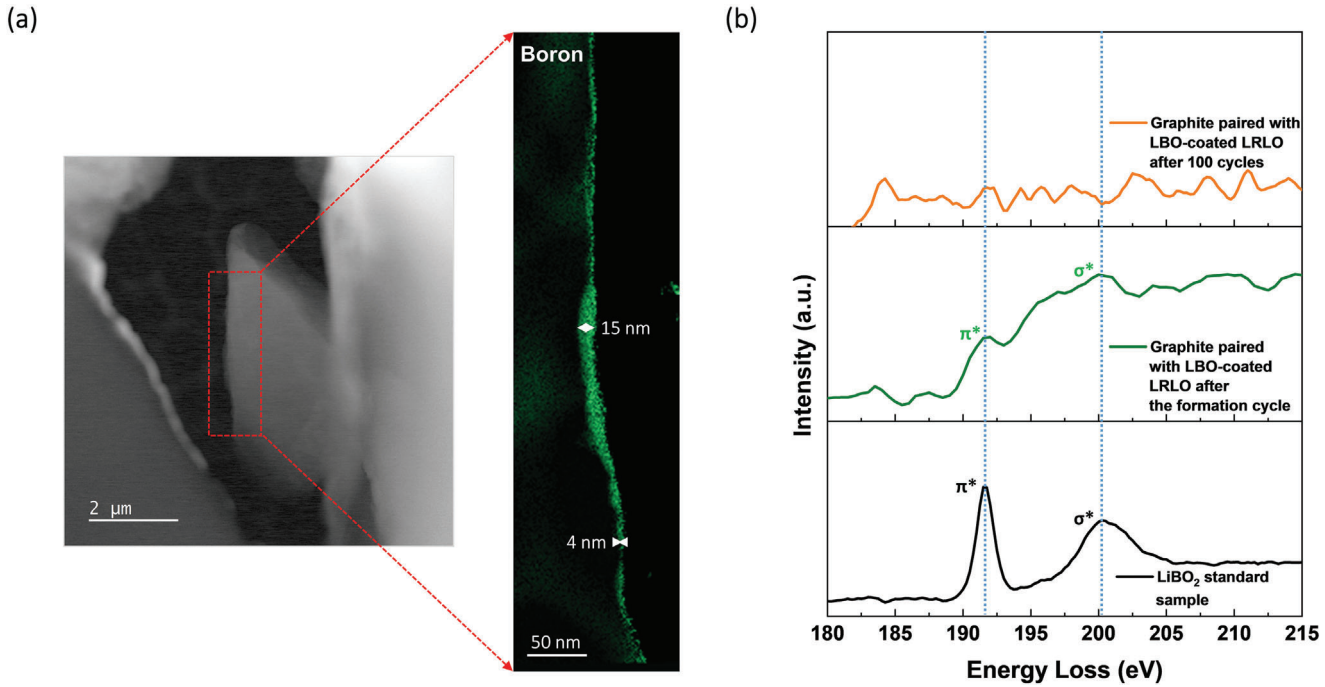

Figure 3. a) STEM-EELS mapping results of graphite paired with LBO-coated LRLO after the formation cycle in the full cell. b) EELS spectra of boron K-edge for cycled graphite and $LiBO_2$ standard sample for comparison.

through the electrolyte and deposits on the anode surface. This process contributes to the formation of the SEI layer, as evidenced by the change in peak intensity ≈3.3 V in dQ/dV plots (Figure 1b). After 100 cycles, like the cathode surface, there is an absence of any observable boron signal on the graphite anode surface. This reinforces that the LBO species can gradually undergo reactions with the electrolyte during extended cycling periods.

2.3. LBO Reactivity with Electrolyte for Performance Improvement

The results obtained from STEM-EELS pinpoint the crucial factor of LBO reactivity with the electrolyte for the improvement of overall cell performance. Due to insufficient electrolyte amount at the coin cell level, single-layer pouch cells were then assembled for cycling evaluation and electrolyte analysis. The uncoated LRLO pouch cell delivers a capacity retention of 79.9% after 70 cycles at a current rate of C/10. In contrast, the LBO-coated LRLO demonstrates a higher retention of 87.4% with a stabilized discharge capacity from ≈40 cycles (Figure S11a, Supporting Information). Additionally, the charge and discharge voltage plot in Figure S11b (Supporting Information) shows that the uncoated LRLO pouch cell has a voltage hysteresis of 0.37 V, while the LBO-coated LRLO reduces the voltage hysteresis to 0.18 V. To avoid excessive electrolyte consumption with prolonged cycling, the pouch cells were stopped at 70 cycles, at which point a clear difference in gas generation (Figure S11c, Supporting Information) was observed. The LRLO pouch cell without LBO coating exhibits evident swelling. This observation underscores the potential of LBO surface modification in reducing the gas generation that arises from the parasitic reactions in the cycled electrolyte at high voltage.[27] Pouch cells of the uncoated LRLO and LBO-coated LRLO were disassembled after the formation cycle and after 70 cycles. Centrifuge tubes were utilized to efficiently extract the electrolyte through rotation at 2000 rpm. The extracted electrolyte was then analyzed by ^{19}F-NMR techniques (Figure S12, Supporting Information).

The presence of BF_4^- anions (**Figure** 4a) is exclusively confirmed in the electrolyte after 70 cycles with LBO-coated LRLO. The formation of BF_4^- is absent even in the initial stage of the LBO-coated LRLO pouch cell, which implies that boron primarily contributes to forming the CEI/SEI layer during the formation cycle. As cycling progresses, boron progressively dissolves into the electrolyte, leading to the formation of the B—F environment. This observation aligns with STEM-EELS results, revealing the absence of boron on the cathode surface after 100 cycles.

To further investigate the reactivity of LBO, an electrolyte comprising 2 wt.% LBO powder dissolved in 1M $LiPF_6$ EC/DMC 3:7 (v%) was examined. For comparison, another electrolyte containing 2 wt.% LiBOB additive was also prepared in the same carbonate baseline electrolyte. In our previous study,[28] the B—F environment was also present in the cycled electrolyte with LiBOB additive, which comes from the reaction between LiBOB and HF acid generated from electrolyte decomposition. Both electrolytes were stored for 1-, 4-, 7-, and 10-days post-preparation, followed by ^{11}B-NMR analysis to trace boron species (Figure 4b). The findings reveal the rapid presence of BF_4^- anions within a day of LBO dissolution. After 10 days, no other boron species, apart from BF_4^-, are detected. This observation implies an immediate reaction of LBO with the fluorine source (PF_6^- anion in the $LiPF_6$ salt) upon dissolution, leading to the formation of the B—F environment. In contrast, when LiBOB is utilized as an electrolyte additive, even after 10 days, a significant portion of the boron persists in the form of BOB^-. The emergence of a

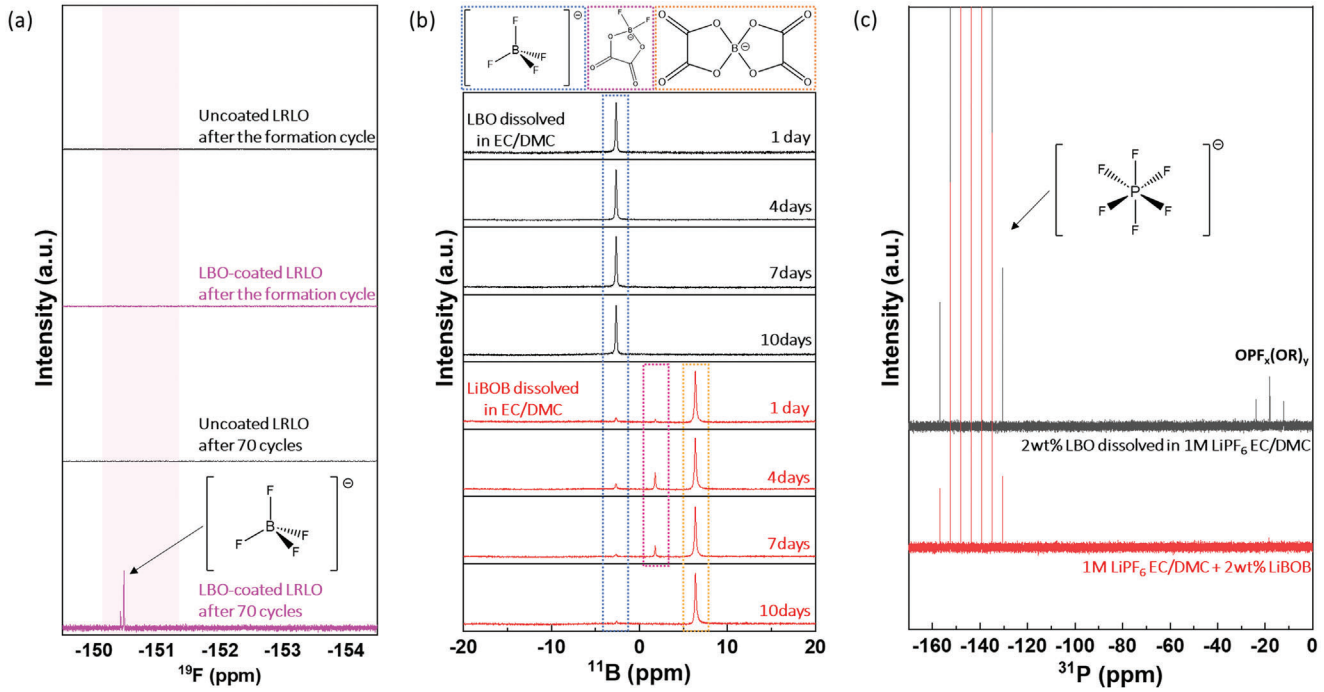

Figure 4. a) ^{19}F-NMR from different electrolyte samples, including cycled electrolytes from the uncoated LRLO and LBO-coated LRLO after the formation cycle and 70 cycles. b) ^{11}B-NMR and c) ^{31}P-NMR from different electrolyte samples, including LBO and LiBOB dissolved into carbonate baseline electrolyte.

small quantity of BF_4^- and $DFOB^-$ in the LiBOB electrolyte after storage is attributed to the disproportionation reaction between fluoride ligands on phosphorus and oxalato ligands on boron (in LiBOB).[29] The considerably higher reactivity of LBO with the carbonate baseline electrolyte is further confirmed by ^{31}P-NMR analysis (Figure 4c). The peak corresponding to PF_6^- in the −160 to −130 ppm range is evident in both electrolytes. However, distinctive peak features ≈−18 ppm associated with the $OPF_x(OR)_y$ organic compounds are observed solely in the electrolyte containing the LBO additive.[30] These organic compounds arise as byproducts of the reaction between LBO and PF_6^- anions in the electrolyte. The distinction in the reaction pathway leading to the formation of the B—F environment between LBO and LiBOB additives is crucial in elucidating the mechanism underlying performance improvement, as detailed below.

Based on all the above findings, the cycling performance improvement of LBO-coated LRLO in full cell is summarized in **Figure 5**. Cycling under high-voltage, the ethylene carbonate (EC) component of the carbonate-based electrolyte undergoes ring opening process (Figure 5a).[31] Carbonate solvents oxidize and decompose, leading to the release of protons. The liberated protons are highly reactive on the cathode surface, binding with the oxygen and generating H_2O. This H_2O then reacts with $LiPF_6$ salt to form HF acid, which is highly corrosive to the cathode and anode surfaces.[32] On the cathode surface, the attack of HF acid causes the dissolution of transition metal, which subsequently redeposits on the anode surface through the electrolyte. The inductively coupled plasma mass spectrometry (ICP-MS) soaking test in Figure S13 (Supporting Information) reveals a significantly higher concentration of Ni and Mn in the graphite when paired with the uncoated LRLO electrode after the formation cycle. The High-angle annular dark-field (HAADF) image (Figure S14, Supporting Information) of the uncoated LRLO is provided for the analysis of the CEI layer after the formation cycle. STEM-EELS mapping reveals distinct clustering of carbon and fluorine, indicating a non-uniform distribution along the surface of primary particles. This observation aligns with the STEM-EDS data presented in Figure S15 (Supporting Information), confirming a similar non-uniform distribution of the SEI layer. Another noteworthy observation is the clear detection of manganese and nickel on the anode surface even after the formation cycle. This indicates that the dissolution and redeposition of transition metals occur even during the formation cycle.

On the other hand, the LBO coating layer on the cathode surface engages in a competitive reaction compared to the $LiPF_6$ hydrolysis process (Figure 5b). As confirmed by ^{31}P-NMR, LBO reacts with PF_6^- to form $LiBF_4$ or phosphorus fluorine oxide species. Given that the reaction between $LiPF_6$ and H_2O occurs simultaneously with the competitive interaction involving LBO, the reaction with H_2O is comparatively suppressed, thereby mitigating HF generation. The comparison of formation energies shows that the generation of B–F species is thermodynamically advantageous. The formation energy of BF_4^- (−1710 kJ mol^{-1})[33] is much lower than that of HF (−273 kJ mol^{-1}),[34] making this reaction more favorable. Moreover, the B—F bond possesses a significantly higher bond energy (613 kJ mol^{-1}) than both H–F (565 kJ mol^{-1}) and P—F (490 kJ mol^{-1}), indicating greater stability of the B–F bond over H–F and P–F bonds.[35] This finding is consistent with the literature, which reports that $LiBF_4$ is more stable than $LiPF_6$.[36] Consequently, in contrast to the uncoated LRLO

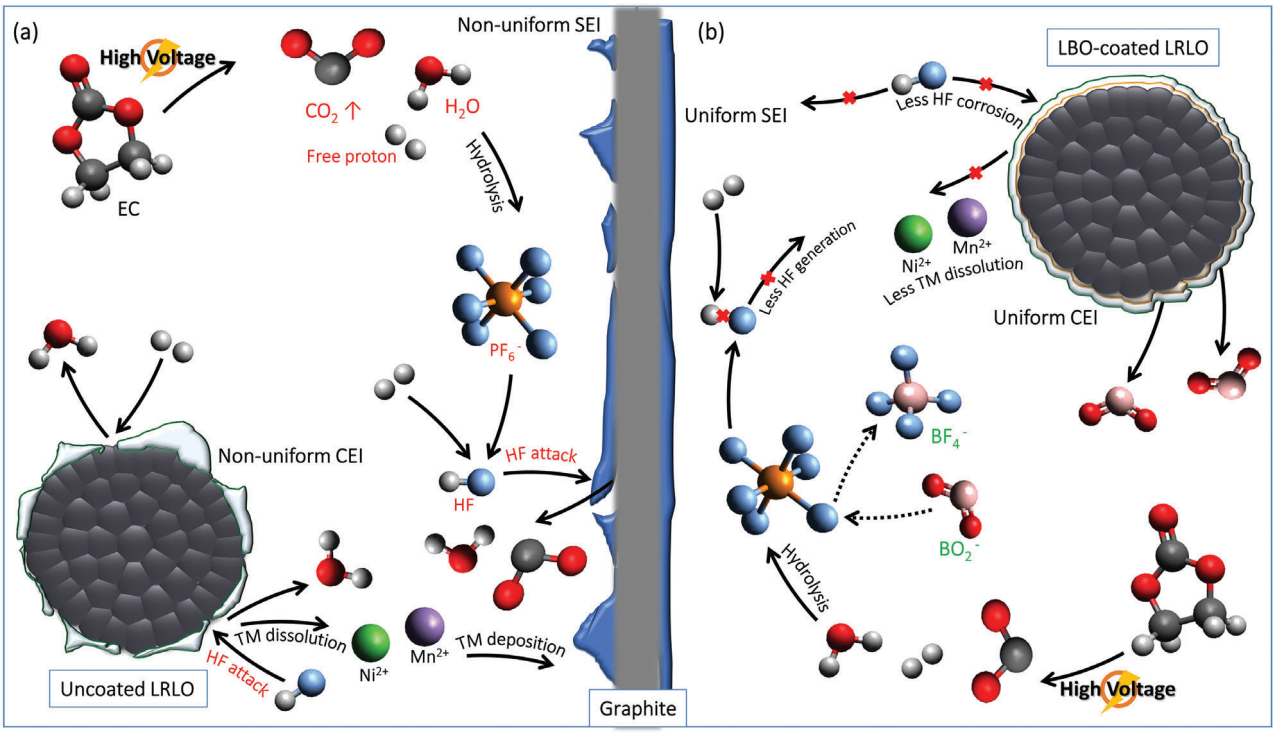

Figure 5. Schematics of performance improvement by LBO-coated LRLO in LRLO/graphite full cell. Reaction pathway for a) uncoated LRLO/graphite full cell and b) LBO-coated LRLO/graphite full cell with carbonate baseline electrolyte.

case, LBO-coated LRLO exhibits a more uniform CEI layer with ≈20 nm in thickness (Figure S16, Supporting Information), indicating the relative attenuation of severe HF acid attacks during cycling. The STEM-EDS data in Figure S17 (Supporting Information) also illustrates a uniform SEI layer, ≈80 nm thick on the graphite anode paired with LBO-coated LRLO after the formation cycle. Transition metals were also detected in this graphite, highlighting that LBO surface modification cannot completely prohibit the dissolution and redeposition of transition metals. However, it is crucial to emphasize that the LBO surface modification plays a significant role in mitigating these effects, as indicated by the results from the ICP-MS analysis (Figure S13, Supporting Information).

The LBO coating cannot prevent the generation of H_2O, which is the intrinsic issue of the EC solvent in a highly oxidative environment;[37] however, the continuous production of HF by PF_6^- can be reduced through the competitive reaction between LBO and PF_6^-. In our previous study,[28] LiBOB was confirmed to serve as the scavenger for the generated HF acid. In order to completely prevent the HF corrosion to the active materials and their interphase, we explore the synergy effect of employing both approaches: incorporating LBO-coated LRLO as the cathode material and introducing LiBOB as the electrolyte additive.

2.4. LBO Coating and LiBOB Additive for Long-Term Cycling Stability

Irrespective of the use of electrolyte additives or surface modification, it shows no obvious capacity degradation during the formation cycle (Figure S18a, Supporting Information). The derivative of the capacity with respect to the cell voltage was then plotted to compare the lithiation/delithiation processes for different cases. Apart from the peak at 3.3 V (corresponding to the CEI/SEI formation), there is no noticeable difference in the dQ/dV versus plots (Figure S18b, Supporting Information). When LiBOB was used as an electrolyte additive or when the surface was modified with LBO, the intensity of the 3.3 V peak in the dQ/dV vs. plots decreases (Figure S18c, Supporting Information).

To assess the synergy effect, a practical-level long-term cycling was conducted. Under the challenging conditions of high voltage, high loading electrode (3 mAh cm^{-2}), and a high current rate (C/3), the LBO-coated LRLO/graphite full cell with LiBOB electrolyte additive exhibits excellent performance, with a capacity retention of 82% after 400 cycles (**Figure 6c**). Furthermore, even under high current rate conditions, a minimal voltage decay of 0.019 V was observed for the discharge process up to 400 cycles (Figure 6d). Based on the performance summary from the published results of the LRLO/graphite full cell (Table S2, Supporting Information), our investigation highlights the optimum cycle performance achieved with a Co-free chemical composition and the highest cathode loading (Figure 6e). Notably, this synergistic effect persists even under elevated temperatures. The high temperature (45 °C) testing results are presented in Figure S19 (Supporting Information). In contrast to the immediate capacity drop of the full cell with the uncoated LRLO cathode (black line), LBO surface modification alone exhibits the capacity to endure for ≈60 cycles (pink line). The inclusion of a 2 wt.% LiBOB electrolyte additive extends the cycling capability beyond 200 cycles. This observation underscores the potential to surmount the challenges

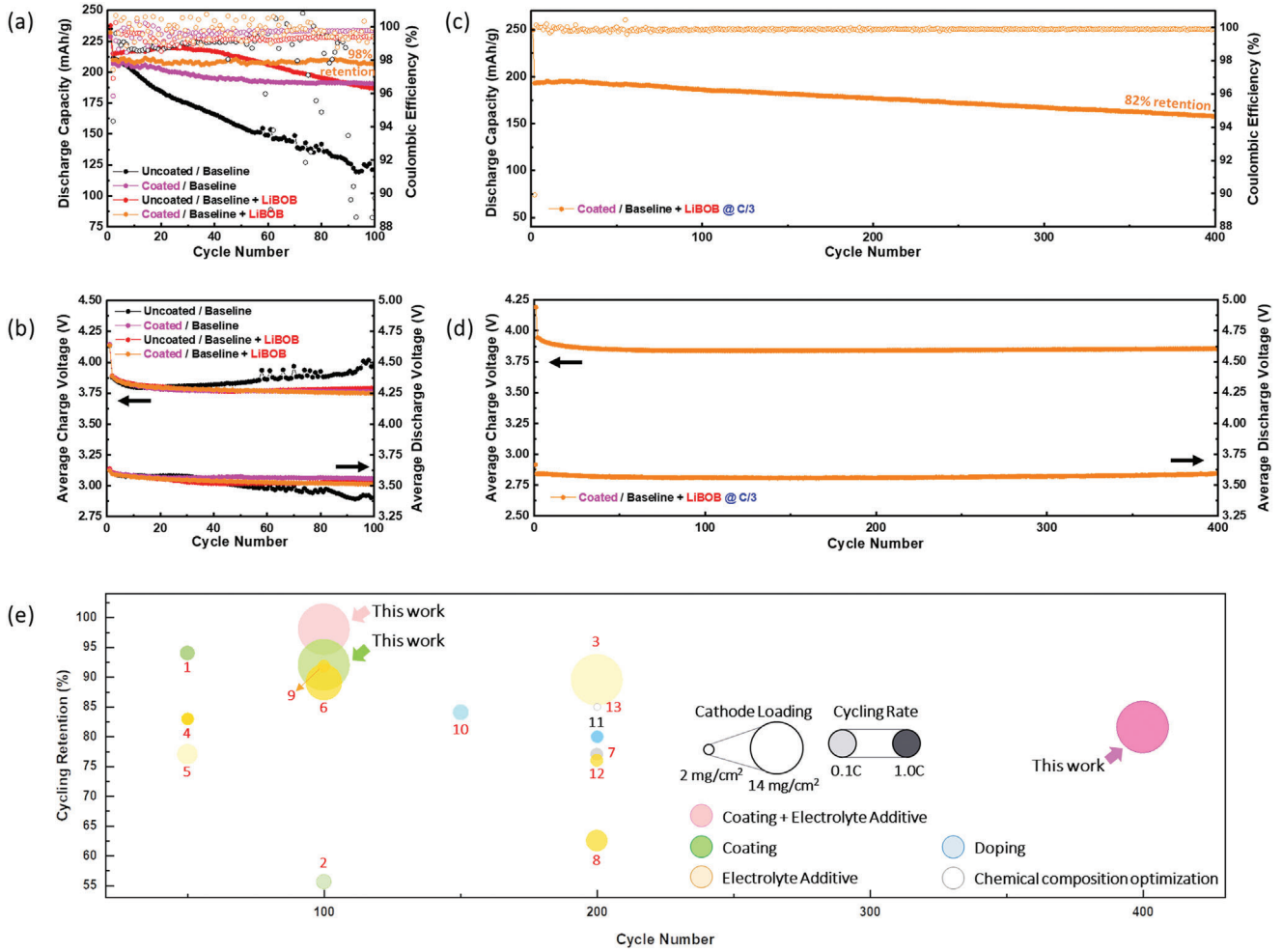

Figure 6. a) Full cells cycling performance comparison with b) the corresponding average charge and discharge voltage in the 2.0–4.55 V window at a current rate of C/10. c) Cycling performance comparison with d) the corresponding average charge and discharge voltage in the 2.0–4.55 V window at a current rate of C/3. e) LRLO/graphite full cell performance summary plot. (The numbers refer to the entries in Table S2 (Supporting Information). Additionally, red numbers indicate Co-containing LRLO cathode materials, while black numbers indicate Co-free LRLO cathode materials.).

associated with cycling at elevated temperatures, another obstacle that has impeded the practical application of LRLO, through strategic utilization of boron chemistry.

3. Conclusion

The oxygen redox products in LRLO, including radical anion complexes, readily engage with carbonate-based electrolytes, causing parasitic side reactions that compromise the cathode material's lattice structure and result in a rapid deterioration of electrochemical performance. This investigation employs boron chemistry to design a strategy for stabilizing the electrode-electrolyte interphase, proving effective in alleviating capacity and voltage decay. The LBO precursor is synthesized using a polyol process, enabling dry coating on the LRLO surface. Under optimized conditions, a uniform LBO coating layer of 15 nm thickness is achieved, contributing to enhanced cycling stability in LRLO/graphite full cells.

The improved full cell performance is attributed to the surface modification by LBO, which protects LRLO's lattice oxygen, and reacts with PF_6^- anions to suppress HF acid generation. This mechanistic understanding is supported by the observed reduction in transition metal dissolution and mitigated interphase corrosion in LBO-coated LRLO. The further incorporation of LiBOB additive, acting as an HF scavenger, results in promising battery performance for industrial-level applications. The full cell with LBO-coated LRLO cathode demonstrates an impressive 82% capacity retention after 400 cycles at a current rate of C/3, with an average discharge voltage drop of 0.019 V. This minimal voltage decay presents a significant opportunity for engineering LRLO materials toward achieving long-term cycling stability.

4. Experimental Section

Sample Preparation: The pristine $Li_{1.222}Ni_{0.349}Mn_{0.651}O_2$ sample (denoted as LRLO) was provided by Umicore. SEM images of the pristine LRLO are presented in Figure S20a–c (Supporting Information), revealing oval-spherical secondary particles with an average size of ≈9 µm. The X-ray diffraction (XRD) pattern was obtained for the structural analysis of the pristine LRLO. Rietveld refinement was applied to the collected XRD data to determine the lattice parameters and site occupancies of the pristine

LRLO sample, as shown in Figure S20d,e (Supporting Information). The XRD pattern can be matched to the R-3m space group, with lattice parameters a = 2.867(6) Å and c = 14.266(4) Å. The refined occupancies reveal a 6.8% Li/Ni mixing between the Li and TM layers. In summary, the LRLO sample exhibits high material purity and a well-organized layered structure with low Li/Ni mixing, establishing it as a reliable baseline material for this study. For coating material synthesis, 0.03 mol of Polyvinylpyrrolidone (PVP) (MW = 50 000) was added to 100 mL of Tetraethylene Glycol (TTEG). 0.015 mol of $LiOH{\cdot}H_2O$ and 0.015 mol of H_3BO_3 were then added into the solution. After 2 h of heating the solution at 80 °C, the products were naturally cooled down, followed by washing in ethanol seven times. After removing moisture in an 80 °C vacuum oven for one day, the dried powder was ground finely using a mortar and pestle, and finally, using a ball mill at 500 rpm for 5 h with ethanol to make the particle size smaller. The obtained LBO precursor (2% in a weight ratio) was then mixed with the LRLO cathode in a Thinky Mixer (Thinky Corporation) at 2000 rpm for 10 min. The well-mixed powder was transferred into the furnace for calcination under different temperatures and dwell time. After calcination, the powder was ground using a mortar and pestle for ≈10 min.

Electrode Preparation: To evaluate the electrochemical performance of LBO-coated LRLO, electrodes using the uncoated and LBO-coated LRLO were prepared, with SPC65 (carbon black, TIMCAL Ltd.) as the conductive agent and HSV900 (PVDF, Arkema Inc.) as the binder, in a mass ratio of 80:10:10 and a cathode loading of 3 mAh cm^{-2}. The mixture was then dissolved in a proper amount of N-methyl-2-pyrrolidone (NMP, ≥ 99%, Sigma–Aldrich) in a Thinky Mixer to form the slurry. The slurry was cast onto Al foil and dried at 80 °C in a vacuum oven overnight, followed by 1 h of drying at elevated temperature of 120 °C. The cathode was punched into discs with a 12.7 mm diameter and a loading of active mass ≈14 mg cm^{-2}. For LRLO/graphite full cells, both CR2032 and pouch cells were assembled. The graphite electrode used in this work was provided by NIMTE with an active material ratio of 94%. For CR2032 full cells, the graphite electrode was punched into discs with a 13 mm diameter, and the designed N/P ratio was ≈1.1. For single layer pouch-type full cells, the cathode size was 44 × 30 mm, and the anode size was 45 × 32 mm. For all the cells, Celgard 2325 was used as the separator. 1M $LiPF_6$ in EC: DMC = 3:7 (vol%) was obtained from Gotion, USA, and is denoted as carbonate baseline electrolyte. All the coin cells were assembled in the Ar-filled glovebox with moisture control (H_2O < 0.5 ppm), and 50 µL of electrolyte was used for each coin cell. The single layer pouch cells were first assembled in the atmosphere without electrolytes. The assembled pouch cells were moved to a heating tray inside the glovebox antechamber and dried at 80 °C overnight under vacuum before the electrolyte injection. After drying, the dry pouches were moved inside the Ar-filled glovebox without air exposure, and 500 µL of electrolyte was injected into each cell. The pouch cells with electrolytes were vacuum sealed inside the glovebox and transferred out for further testing.

Electrochemical Performance Evaluation: After assembling, the coin cell (CR2032) and pouch cell full cells were evaluated by cycling at a rate of C/10 (where 1C is 270 mAh g^{-1}) after the formation cycle at a current rate C/20. The electrochemical performances of all the cells were tested either by Neware Battery Test System (Neware Technology Ltd., China) or Arbin BT2000 instruments (Arbin instrument, USA).

Characterizations: FEI Apreo was applied with 5 kV as the accelerating voltage and 0.1 nA as the beam current for the SEM analysis. A backscattered electron imaging technique was applied to verify the uniformity of the LBO surface modification layer on LRLO, especially for large-area coating uniformity evaluation. The microscope detector was first changed to T1 mode, which was extremely sensitive to backscattered electrons. Then, the accelerated voltage was lowered to detect the surface information. The contrast gradually appeared when lowering the accelerated voltage from 5 kV to 200 V, while the optimized voltage was 500 to 1000 V to acquire clear images. A Thermofisher Talos F200X G2 transmission electron microscope, equipped with a Ceta camera and operated at 200 kV, was used to acquire STEM-EELS and STEM-EDS data. To minimize possible electron beam irradiation effects, EELS spectra presented in this work were acquired from areas without pre-beam irradiation. ICP-MS analysis was performed with a Thermo iCAP RQ ICP-MS to analyze the elemental concentration in fresh and cycled electrolytes. The ^{11}B, ^{19}F, and ^{31}P-NMR measurements of the electrolyte samples were performed with a JEOL ECA 500 spectrometer. Liquid NMR samples were prepared by adding 10 µL of electrolyte to 600 µL of DMSO-D6 solution, and 50 µL of α, α, α-Trifluorotoluene was added to each sample as the reference and sealed in an NMR tube inside the Ar-filled glovebox for further measurement. The NMR spectrums were analyzed with MestReNova. All spectra were calibrated with α, α, α-Trifluorotoluene at −63.72 ppm. FT-IR spectra were collected using Nicolet 6700 Fourier transform infrared spectrometer. Approximately 5−10 mg of LRLO was dried at 80 °C for at least 12 h before the FT-IR analysis. The electronic conductivity was determined using the direct current polarization method using a Biologic SP-200 impedance analyzer by applying a bias of 10 mV for 1 h and extracting the steady-state leakage current.

Supporting Information

Supporting Information is available from the Wiley Online Library or from the author.

Acknowledgements

This work was supported by Umicore. The authors thank Wendy Zhou for her invaluable advice. STEM-EELS in this work were performed at the Nano3 of UCSD, a member of the National Nanotechnology Coordinated Infrastructure, which is supported by the National Science Foundation (Grant ECCS-1542148). The ICP-MS was conducted at the Environmental and Complex Analysis Laboratory (ECAL) in the Chemistry and Biochemistry department at UC San Diego. The NMR in this work was conducted at the Chemistry NMR facility at UC San Diego. The authors are grateful for Umicore providing the LRLO cathode materials used in the research. The authors thank Prof. Zhaoping Liu's group from Ningbo Institute of Materials Technology & Engineering (NIMTE) for providing the graphite anode. Finally, I dedicate this thesis to my mother.

Conflict of Interest

The authors declare no conflict of interest.

Author Contributions

N.P., M.Z., and Y.S.M. conceived the idea. N.P. and M.Z. designed the experiments. N.P. synthesized the organic nano-sized boron precursor and performed LBO-coating on LRLO cathode material. N.P. collected and analyzed the data for SEM-EDS, ICP-MS, liquid NMR, FT-IR, and electrochemical performances. B.H. collected and processed the data for STEM-EELS and STEM-EDS. All authors discussed the results and contributed to the manuscript. All authors have approved the final version of the manuscript.

Data Availability Statement

The data that support the findings of this study are available from the corresponding author upon reasonable request.

Keywords

high voltage, lithium borate (LBO), lithium rich layered oxide (LRLO), Mn-rich, surface modification

Received: May 4, 2024
Revised: September 6, 2024
Published online:

[1] M. Armand, P. Axmann, D. Bresser, M. Copley, K. Edström, C. Ekberg, D. Guyomard, B. Lestriez, P. Novák, M. Petranikova, W. Porcher, S. Trabesinger, M. Wohlfahrt-Mehrens, H. Zhang, *J. Power Sources* **2020**, *479*, 228708.
[2] M. D. Radin, S. Hy, M. Sina, C. Fang, H. Liu, J. Vinckeviciute, M. Zhang, M. S. Whittingham, Y. S. Meng, A. van der Ven, *Adv. Energy Mater.* **2017**, *7*, 1602888.
[3] F. Wu, G. T. Kim, T. Diemant, M. Kuenzel, A. R. Schür, X. Gao, B. Qin, D. Alwast, Z. Jusys, R. J. Behm, D. Geiger, U. Kaiser, S. Passerini, *Adv. Energy Mater.* **2020**, *10*, 2001830.
[4] B. Zhang, L. Wang, X. Wang, S. Zhou, A. Fu, Y. Yan, Q. Wang, Q. Xie, D. Peng, Y. Qiao, S. G. Sun, *Energy Storage Mater.* **2022**, *53*, 492.
[5] M. Zhang, H. Liu, Z. Liu, C. Fang, Y. S. Meng, *ACS Appl. Energy Mater.* **2018**, *1*, 3369.
[6] Y.-L. Heng, Z.-Y. Gu, J.-Z. Guo, X.-T. Yang, X.-X. Zhao, X.-L. Wu, *Energy Materials* **2022**, *2*, 200017.
[7] M. Zhang, D. A. Kitchaev, Z. Lebens-Higgins, J. Vinckeviciute, M. Zuba, P. J. Reeves, C. P. Grey, M. S. Whittingham, L. F. J. Piper, A. van der Ven, Y. S. Meng, *Nat. Rev. Mater.* **2022**, *7*, 522.
[8] A. Singer, M. Zhang, S. Hy, D. Cela, C. Fang, T. A. Wynn, B. Qiu, Y. Xia, Z. Liu, A. Ulvestad, N. Hua, J. Wingert, H. Liu, M. Sprung, A. v. Zozulya, E. Maxey, R. Harder, Y. S. Meng, O. G. Shpyrko, *Nat. Energy* **2018**, *3*, 641.
[9] Y. Li, M. J. Zuba, S. Bai, Z. W. Lebens-Higgins, B. Qiu, S. Park, Z. Liu, M. Zhang, L. F. J. Piper, Y. S. Meng, *Energy Storage Mater.* **2021**, *35*, 99.
[10] S. Hy, H. Liu, M. Zhang, D. Qian, B. J. Hwang, Y. S. Meng, *Energy and Environm. Sci.* **2016**, *9*, 1931.
[11] T. Zhao, S. Chen, R. Chen, L. Li, X. Zhang, M. Xie, F. Wu, *ACS Appl. Mater. and Interfaces* **2014**, *6*, 21711.
[12] X. Zhang, I. Belharouak, L. Li, Y. Lei, J. W. Elam, A. Nie, X. Chen, R. S. Yassar, R. L. Axelbaum, *Adv. Energy Mater.* **2013**, *3*, 1299.
[13] S. Y. Kim, C. S. Park, S. Hosseini, J. Lampert, Y. J. Kim, L. F. Nazar, *Adv. Energy Mater.* **2021**, *11*, 2100552.
[14] N. R. Park, Y. Li, W. Yao, M. Zhang, B. Han, C. Mejia, B. Sayahpour, R. Shimizu, B. Bhamwala, B. Dang, S. Kumakura, W. Li, Y. S. Meng, *Adv. Funct. Mater.* **2023**, *34*, 2312091.
[15] J. Zheng, M. Gu, J. Xiao, B. J. Polzin, P. Yan, X. Chen, C. Wang, J. G. Zhang, *Chem. Mater.* **2014**, *26*, 6320.
[16] F. Wu, X. Zhang, T. Zhao, L. Li, M. Xie, R. Chen, *ACS Appl. Mater. and Interfaces* **2015**, *7*, 3773.
[17] S. J. Shi, J. P. Tu, Y. Y. Tang, Y. Q. Zhang, X. Y. Liu, X. L. Wang, C. D. Gu, *J. Power Sources* **2013**, *225*, 338.
[18] C. H. Jo, D. H. Cho, H. J. Noh, H. Yashiro, Y. K. Sun, S. T. Myung, *Nano Res.* **2015**, *8*, 1464.
[19] J. Jiang, Y. Li, J. Liu, X. Huang, C. Yuan, X. W. Lou, *Adv. Mater.* **2012**, *24*, 5166.
[20] W. Wang, Z. Yin, J. Wang, Z. Wang, X. Li, H. Guo, *J. Alloys Compd.* **2015**, *651*, 737.
[21] L. Zhou, Z. Yin, H. Tian, Z. Ding, X. Li, Z. Wang, H. Guo, *Appl. Surf. Sci.* **2018**, *456*, 763.
[22] W. Liu, P. Oh, X. Liu, S. Myeong, W. Cho, J. Cho, *Adv. Energy Mater.* **2015**, *5*, 1500274.
[23] L. J. Zhou, Z. L. Yin, Z. Y. Ding, X. H. Li, Z. X. Wang, H. J. Guo, *Ionics* **2018**, *24*, 2533.
[24] H. Liu, D. Qian, M. G. Verde, M. Zhang, L. Baggetto, K. An, Y. Chen, K. J. Carroll, D. Lau, M. Chi, G. M. Veith, Y. S. Meng, *ACS Appl. Mater. and Interfaces* **2015**, *7*, 19189.
[25] H. Sauer, R. Brydson, P. N. Rowley, W. Engel, J. M. Thomas, *Ultramicroscopy* **1993**, *49*.
[26] G. Lelong, L. Cormier, L. Hennet, F. Michel, J. P. Rueff, J. M. Ablett, G. Monaco, *J. Non-Cryst. Solids* **2017**, *472*, 1.
[27] W. Yao, M. Chouchane, W. Li, S. Bai, Z. Liu, L. Li, A. X. Chen, B. Sayahpour, R. Shimizu, G. Raghavendran, M. A. Schroeder, Y. T. Chen, D. H. S. Tan, B. Sreenarayanan, C. K. Waters, A. Sichler, B. Gould, D. J. Kountz, D. J. Lipomi, M. Zhang, Y. S. Meng, *Energy and Environm. Sci.* **2023**, *16*, 1620.
[28] Y. Li, W. Li, R. Shimizu, D. Cheng, H. N. Nguyen, J. Paulsen, S. Kumakura, M. Zhang, Y. S. Meng, *Adv. Energy Mater.* **2022**, *12*, 2103033.
[29] A. Xiao, L. Yang, B. L. Lucht, *Electrochem. Solid-State Lett.* **2007**, *10*, 241.
[30] Y. Dong, J. Demeaux, Y. Zhang, M. Xu, L. Zhou, A. D. MacIntosh, B. L. Lucht, *J. Electrochem. Soc.* **2017**, *164*, A128.
[31] M. Metzger, B. Strehle, S. Solchenbach, H. A. Gasteiger, *J. Electrochem. Soc.* **2016**, *163*, A1219.
[32] W. Li, D. Cheng, R. Shimizu, Y. Li, W. Yao, G. Raghavendran, M. Zhang, Y. S. Meng, *Energy Storage Mater.* **2022**, *49*, 77.
[33] V. Aravindan, J. Gnanaraj, S. Madhavi, H. K. Liu, *Chemistry – A European Journal* **2011**, *17*, 14326.
[34] J. D. Cox, D. D. Wagman, V. A. Medvedev, CODATA Key Values for Thermodynamics, Hemisphere Publishing Corp, New York **1989**.
[35] T. L. Cottrell, *The Strengths of Chemical Bonds*, Butterworths Scientific Publications, London **1958**.
[36] L. D. Ellis, I. G. Hill, K. L. Gering, J. R. Dahn, *J. Electrochem. Soc.* **2017**, *164*, A2426.
[37] M. Liu, J. Vatamanu, X. Chen, L. Xing, K. Xu, W. Li, *ACS Energy Lett.* **2021**, *6*, 2096.